Chemical Geology 479 (2018) 166–175

Contents lists available at ScienceDirect

Chemical Geology

journal homepage: www.elsevier.com/locate/chemgeo

Determination of $Fe^{3+}/\Sigma Fe$ of XANES basaltic glass standards by Mössbauer spectroscopy and its application to the oxidation state of iron in MORB

Hongluo L. Zhang[a,*], Elizabeth Cottrell[b], Peat A. Solheid[c], Katherine A. Kelley[d], Marc M. Hirschmann[e]

[a] CAS Key Laboratory of Crust-Mantle Materials and Environments, School of Earth and Space Sciences, University of Science and Technology of China, Hefei 230026, China
[b] National Museum of Natural History, Smithsonian Institution, Washington, DC 20560, USA
[c] Institute for Rock Magnetism, University of Minnesota, Minneapolis, MN 55455, USA
[d] Graduate School of Oceanography, University of Rhode Island, Narragansett, RI 02882, USA
[e] Department of Earth Sciences, University of Minnesota, Minneapolis, MN 55455, USA

ARTICLE INFO

Keywords:
Mössbauer spectroscopy
MORB
Recoilless fraction
$Fe^{3+}/\Sigma Fe$
XANES
Oxygen fugacity

ABSTRACT

To improve the accuracy of X-ray absorption near-edge structure (XANES) calibrations for the $Fe^{3+}/\Sigma Fe$ ratio in basaltic glasses, we reevaluated the $Fe^{3+}/\Sigma Fe$ ratios of glasses used as standards by Cottrell et al. (2009), and available to the community (NMNH catalog #117393). Here we take into account the effect of recoilless fraction on the apparent $Fe^{3+}/\Sigma Fe$ ratio measured from room temperature Mössbauer spectra in that original study. Recoilless fractions were determined from Mössbauer spectra collected from 40 to 320 K for one basaltic glass, AII_25, and from spectra acquired at 10 K for the 13 basaltic glass standards from the study of Cottrell et al. (2009). The recoilless fractions, f, of Fe^{2+} and Fe^{3+} in glass AII_25 were calculated from variable-temperature Mössbauer spectra by a relative method (RM), based on the temperature dependence of the absorption area ratios of Fe^{3+} and Fe^{2+} paramagnetic doublets. The resulting correction factor applicable to room temperature determinations (C_{293}, the ratio of recoilless fractions for Fe^{3+} and Fe^{2+}) is 1.125 ± 0.068 (2σ). Comparison of the spectra at 10 K for the 13 basaltic glasses with those from 293 K suggests C_{293} equal to 1.105 ± 0.015 (2σ). Although the 10 K estimate is more precise, the relative method determination is believed to be more accurate, as it does not depend on the assumption that recoilless fractions are equal at 10 K. Applying the effects of recoilless fraction to the relationship between Mössbauer-determined $Fe^{3+}/\Sigma Fe$ ratios and revised average XANES pre-edge centroids for the 13 standard glasses allows regression of a new calibration of the relationship between the Fe XANES pre-edge centroid energy and the $Fe^{3+}/\Sigma Fe$ ratio of silicate glass. We also update the calibration of Zhang et al. (2016) for andesites and present a more general calibration for mafic glasses including both basaltic and andesitic compositions. Recalculation of $Fe^{3+}/\Sigma Fe$ ratios for the mid-ocean ridge basalt (MORB) glasses analyzed previously by XANES by Cottrell and Kelley (2011) results in an average $Fe^{3+}/\Sigma Fe$ ratio for MORB of 0.143 ± 0.008 (1σ), taking into account only analytical precision, and 0.14 ± 0.01(1σ), taking into account uncertainty on the value of C_{293}. This revised average is lower than the average of 0.16 ± 0.01 given by Cottrell and Kelley (2011). The revised average oxygen fugacity for MORB based on the database of Cottrell and Kelley (2011) is −0.18 ± 0.16 log units less than the quartz-fayalite-magnetite buffer of Frost (1991) at 100 kPa (ΔQFM = −0.18 ± 0.16).

1. Introduction

Analyses of the $Fe^{3+}/\Sigma Fe$ ratio of mafic glasses provide essential information on the redox state of the mantle (Christie et al., 1986; Carmichael, 1991; McCammon and Kopylova, 2004; Bézos and Humler, 2005; Kelley and Cottrell, 2009; Cottrell and Kelley, 2011), and on redox changes associated with crustal differentiation (Kelley and Cottrell, 2012; Brounce et al., 2014; Grocke et al., 2016) and with magmatic degassing (Crabtree and Lange, 2012; Kelley and Cottrell, 2012; de Moor et al., 2013; Moussallam et al., 2014, 2016; Waters and Lange, 2016). Owing to the availability and refinement of X-ray absorption near-edge structure (XANES) analyses to achieve high precision and spatial resolution (Berry et al., 2003; Wilke et al., 2005; Cottrell et al., 2009; Dyar et al., 2016; Fiege et al., 2017), studies of

* Corresponding author.
E-mail address: hongluo@ustc.edu.cn (H.L. Zhang).

https://doi.org/10.1016/j.chemgeo.2018.01.006
Received 26 June 2017; Received in revised form 23 November 2017; Accepted 5 January 2018
Available online 06 January 2018

$Fe^{3+}/\Sigma Fe$ ratios in natural glasses have proliferated in recent years. The widespread adoption of XANES for $Fe^{3+}/\Sigma Fe$ ratio determinations of natural glasses makes it essential that attention be paid to the accuracy of this relatively new technique. Because quantitative XANES analysis of Fe oxidation state derives from calibration against independently-known standards, this in turn requires careful attention to the accuracy of methods used in the characterization of standard reference materials.

Particularly important constraints on redox of the mantle and crust derive from the $Fe^{3+}/\Sigma Fe$ ratios of mid-ocean ridge basalt (MORB) glasses, which define the oxidation state of the primitive oceanic crust and are related directly to the oxygen fugacity (fO_2) of the sub-oceanic mantle (Carmichael and Ghiorso, 1986; Christie et al., 1986; Ballhaus, 1993; Bézos and Humler, 2005; Frost and McCammon, 2008; Cottrell and Kelley, 2011). From wet chemical analyses, Christie et al. (1986) found a mean value of 0.07 ± 0.03 (1σ) for a global suite of 87 MORB glasses, whereas 105 MORB glass analyses by Bézos and Humler (2005) produced an average of 0.12 ± 0.02 (1σ). In contrast, XANES analyses of 103 MORB glasses, calibrated via Mössbauer spectroscopy, have a yet greater average value, 0.16 ± 0.01 (1σ) (Cottrell and Kelley, 2011). These distinct ratios convert to more than an order of magnitude difference in the estimated oxygen fugacity, fO_2, of primitive MORB magmas and their source, which in turn amounts to significant differences in the expected depth extent of carbonate-induced melting and metal precipitation in the mantle (Stagno and Frost, 2010; Stagno et al., 2013) and in reconstructed mantle temperatures through determination of FeO*-MgO systematics (Herzberg and Asimow, 2015; Putirka, 2016).

Possible causes for differences in average MORB glass $Fe^{3+}/\Sigma Fe$ ratios determined by wet chemistry (Christie et al., 1986; Bézos and Humler, 2005) and XANES (Cottrell and Kelley, 2011) include incorporation of olivine microphenocrysts in bulk wet chemical aliquots, the interference of additional redox couples during wet chemical dissolution, or systematic differences between the room temperature Mössbauer-based XANES calibration and wet-chemistry (Cottrell and Kelley, 2011). XANES determinations, although highly precise, depend on standardization against materials of known $Fe^{3+}/\Sigma Fe$ ratio, and so are only as accurate as the methods used for calibration.

In many cases, the $Fe^{3+}/\Sigma Fe$ ratios of XANES standards have been independently determined by Mössbauer spectroscopy (Berry et al., 2003; Wilke et al., 2005; Cottrell et al., 2009; Zhang et al., 2016; Alderman et al., 2017). Accurate determination of $Fe^{3+}/\Sigma Fe$ ratios in silicate glasses by Mössbauer spectroscopy is the subject of a long-standing controversy, in part owing to debate as to the influence of recoilless fraction on the area ratios of room temperature (RT) Mössbauer absorption doublets associated with paramagnetic Fe^{2+} and Fe^{3+} in silicate glasses (Mysen et al., 1985; Dyar et al., 1987; Lange and Carmichael, 1989; Ottonello et al., 2001; Righter et al., 2013; Zhang et al., 2015). Recoilless fraction (f) for each kind of iron species, which is the ratio of γ-ray reacted iron ions and total iron ions, therefore, it is mainly controlled by the lattice dynamics in the samples. Both theoretical considerations of bond strengths (Chen and Yang, 2007) and abundant evidence from minerals (Leider and Pipkorn, 1968; Seifert and Olesch, 1977; Chambaere et al., 1984; De Grave et al., 1984; De Grave et al., 1985; Vandenberghe et al., 1986; Bowen et al., 1989; Ellwood et al., 1989; Persoons, 1990; De Grave and Van Alboom, 1991; de Bakker, 1994; Fei et al., 1994; McCammon et al., 1995; Van Alboom and De Grave, 1996; De Grave et al., 1998; McCammon, 1998; Eeckhout et al., 1999; Eeckhout et al., 2000; Eeckhout and De Grave, 2003; Dyar et al., 2008; Dyar et al., 2012; Dyar et al., 2013) demonstrate that RT Mössbauer analyses are likely to overestimate $Fe^{3+}/\Sigma Fe$ ratios of Fe-bearing silicates unless a correction for recoilless fraction is applied. This concept is illustrated in Fig. 1, which shows a compilation of published room-temperature recoilless fractions ($f_{293-300}$) of Fe^{3+} and Fe^{2+} from silicate and oxide minerals. To minimize the effect from large collection of a single phase, we use the averaged $f_{293-300}$ from literature for the same phase, and all values have been listed in Table S1

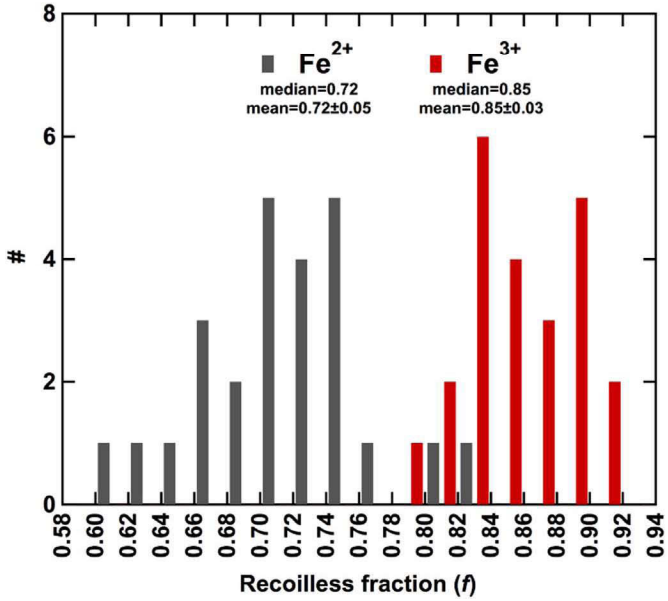

Fig. 1. Values of Mössbauer recoilless fraction for Fe^{3+}, $f(Fe^{3+})_{293-300}$, and Fe^{2+}, $f(Fe^{2+})_{293-300}$, in silicate and oxide minerals at room temperature compiled from previously published studies. To minimize the bias from large dataset of single phase, we use the average number for each phase and the values have been listed in Table S1. Because bond strengths for Fe^{3+} are generally stronger than for Fe^{2+}, values of Mössbauer $f(Fe^{3+})_{293-300}$ are mostly greater than $f(Fe^{2+})_{293-300}$, such that room temperature Mössbauer analyses of materials with both Fe^{3+} and Fe^{2+} will tend to overestimate the fraction of Fe^{3+} unless the effects of recoilless fraction are quantified. The ratio of the mean values of $f(Fe^{3+})_{293-300}$ and $f(Fe^{2+})_{293-300}$, which can be taken as the approximate value of C_{293} typical for silicate and oxide minerals, is 1.16 ± 0.10.

(Leider and Pipkorn, 1968; Seifert and Olesch, 1977; Chambaere et al., 1984; De Grave et al., 1984; De Grave et al., 1985; Vandenberghe et al., 1986; Bowen et al., 1989; Ellwood et al., 1989; Persoons, 1990; De Grave and Van Alboom, 1991; de Bakker, 1994; Fei et al., 1994; McCammon et al., 1995; Van Alboom and De Grave, 1996; De Grave et al., 1998; McCammon, 1998; Eeckhout et al., 1999; Eeckhout et al., 2000; Eeckhout and De Grave, 2003; Dyar et al., 2008; Dyar et al., 2012; Dyar et al., 2013).The larger values of f_{293} for Fe^{3+} compared to Fe^{2+} require a greater magnitude of Mössbauer absorption per atom of absorber. However, the influence of recoilless fraction on the $Fe^{3+}/\Sigma Fe$ ratios of silicate glasses is comparatively subtle, in part because glasses produce broadened line shapes that degrade analytical precision. As reviewed by Zhang et al. (2015), characterization efforts have not always produced statistically resolvable effects, though Mysen (2006) resolved f_{Fe3+}/f_{Fe2+} from 1.04 to 1.20 for aluminosilicate glasses from Mössbauer measurements made at 77 and 298 K. At the time of publication, Cottrell et al. (2009) had only room-temperature Mössbauer spectra available with which to calibrate their now widely-applied XANES calibration for basaltic glasses. If a recoilless fraction for such glasses can be resolved, then $Fe^{3+}/\Sigma Fe$ ratios determined by XANES with this calibration, including the values for MORB presented by Cottrell and Kelley (2011), would shift to lower values.

Recently, Zhang et al. (2015) made a detailed analysis of low temperature Mössbauer spectra of an andesitic glass, and were able to resolve recoilless fraction effects that exceed the analytical limit of detection. In this contribution, we update that calibration and conduct a similar investigation for glass of basaltic composition.

2. Mössbauer spectra collection

Cryogenic (10 K) Mössbauer spectra of basaltic glasses from Cottrell et al. (2009) were collected using constant acceleration transmission mode with a nominal 50 mCi ^{57}Co source at Geophysical Laboratory, Carnegie Institution of Washington. A pure Fe foil calibrant at room

temperature (293 K) was applied. Room temperature Mössbauer spectra on these glasses were also collected with the same protocols, as reported in Cottrell et al. (2009).

Additional Mössbauer spectra of one of these glasses, AII_25, quenched from a 100 kPa gas mixing furnace at 2.47 log units above the quartz-fayalite-magnetite (QFM) buffer, as reported in Cottrell et al. (2009), were collected at the Institute for Rock Magnetism, University of Minnesota. Data were collected at 40–320 K using a constant acceleration Mössbauer spectrometer [Web Research (currently SeeCo)] equipped with a Janis Nitrogen shielded helium dewar, using a ^{57}Co/Rh source and calibrated against a pure Fe foil at room temperature (293 K). Data collection procedures were the same as described in Zhang et al. (2015). Sample mounts consisted of a compressed powder pellet of approximately circular shape and a diameter of 12.7 mm, made from powdered AII_25 glass evenly mixed with cellulose in a 1:1 ratio. The absorber thickness was adjusted for an absorber density of ~8 mg/cm^2 Fe.

3. Results

All Mössbauer spectra on sample AII_25 and glasses analyzed at 10 K were fitted with a 2D distribution Extended Voigt based fitting (xVBF) method with the RECOIL software package (Lagarec and Rancourt, 1997). There is no resolvable evidence of sextets in any spectra, and so at all temperatures paramagnetic Fe^{2+} and Fe^{3+} dominate the Fe ions in the glass. Spectra were fit using the process described in Zhang et al. (2015). Nominal (uncorrected) $Fe^{3+}/\Sigma Fe$ ratios were calculated from the ratio of absorption areas of Fe^{3+} doublets relative to the whole resonant absorption area. The chi-squared goodness-of-fit statistic (χ^2) is < 3 for all fits.

To ensure consistency between the fitting methods applied in this work and those of Cottrell et al. (2009), Mössbauer spectra collected for basaltic glasses at room temperature (293 K) by Cottrell et al. (2009) and originally fit using the method of Alberto et al. (1996) were also refit with the RECOIL software package (Lagarec and Rancourt, 1997) with the same procedure described above and in Zhang et al. (2015). The methods of Alberto et al. (1996) and xVBF both fit the hyperfine parameters and those hyperfine parameters then generate the absorption envelope. Because these two methods are based on the Gaussian distribution of Lorentzian line shapes, a single doublet can accommodate asymmetry in the envelope. We list new fit parameters in Table S2 and show an example of a RT xVBF fit in Fig. S1. The resulting $Fe^{3+}/\Sigma Fe$ ratios, uncorrected for recoilless fraction effects, are consistent with the results from Cottrell et al. (2009) (Fig. S2).

Cryogenic (10 K) Mössbauer spectra of basaltic glasses have more broadened line-shapes than spectra from the same samples collected at room temperature, as has been observed previously (Dyar et al., 2012; Zhang et al., 2015). Spectra consisted of two quadrupole doublets, one each originating from paramagnetic ferric iron and ferrous iron, and these were fit following the procedure of Zhang et al. (2015). Cryogenic Mössbauer spectra were collected at 4 mm/s scale, which causes a short base line on the high velocity side (Fig. S1). Leaving the hyperfine parameters unconstrained during fitting, three spectra (LW_-20, All_-15 and All_-05) yielded $Fe^{3+}/\Sigma Fe$ ratios inconsistent with those derived from the RT Mössbauer spectra on the same samples. Moreover, the Lorentzian Half Width at Half Maximum (HWHM) in these unconstrained fits was < 0.1 mm/s, which is lower than expected and reached the minimum limit allowed within the RECOIL software package. Unconstrained fits of the RT spectra of reduced glasses consistently yielded CS ~0.6. Guided by this, we fixed CS near ~0.6 mm/s when fitting the cryogenic spectra. In this fitting scenario, the Lorentzian HWHM were > 0.1 mm/s (as expected), χ^2 values are < 3, and the $Fe^{3+}/\Sigma Fe$ ratios were consistent with those found at RT. We show example spectra with constrained and unconstrained fits in Fig. S1 and list the resulting Mössbauer parameters in Table S3.

The absorption areas of Mössbauer doublets produced by Fe^{3+} and Fe^{2+} in an analyte ($AA(Fe^{3+})_T$, $AA(Fe^{2+})_T$) are related to the abundances of the ions ($N(Fe^{3+})$, $N(Fe^{2+})$) and the recoilless fraction (f_T) of each ion, according to

$$\frac{AA(Fe^{3+})_T}{AA(Fe^{2+})_T} = C_T \frac{N(Fe^{3+})}{N(Fe^{2+})} \quad (1)$$

where C_T, the correction factor, equals $f(Fe^{3+})_T/f(Fe^{2+})_T$, and the T subscripts highlight quantities that are temperature-dependent. The fractions of ferric and ferrous iron in materials are commonly considered in terms of the $Fe^{3+}/\Sigma Fe$ ratio, rather than the Fe^{3+}/Fe^{2+} ratio as given in Eq. (1). Given an accurate value of the correction factor at room temperature, C_{293}, the true $Fe^{3+}/\Sigma Fe$ ratio in the sample (denoted in equations below as y) is related to the apparent $Fe^{3+}/\Sigma Fe$ ratio measured by uncorrected Mössbauer spectra collected at room temperature (y_{293}) by

$$\frac{Fe^{3+}}{\Sigma Fe} = y = \frac{y_{293}}{[y_{293} + C_{293}(1 - y_{293})]}. \quad (2)$$

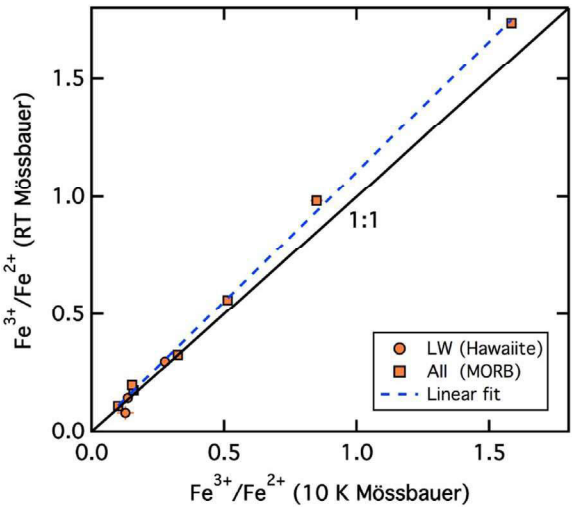

Fig. 2. Comparison of Fe^{3+}/Fe^{2+} ratios determined for standard basaltic glasses by Mössbauer spectroscopy at room temperature (293 K, RT) and 10 K. If the Fe^{3+}/Fe^{2+} ratio determined at 10 K is taken to be the accurate value unaffected by effects of recoilless fraction, then C_{293} (Eq. (1)) is the mean ratio of the determined Fe^{3+}/Fe^{2+}, which is resolved through a weighted least squares regression using 2σ weights for both room temperature and 10 K determinations and a Levenberg-Marquart algorithm. The resulting linear relationship (y = ax) has a slope of 1.105 ± 0.015 and an r^2 of 0.997. To maintain internal consistency, the $Fe^{3+}/\Sigma Fe$ ratios resulting from re-determination of the *RT* Mössbauer fits listed in Table S2 are employed. The error bars reflect precision (2 σ) though for some data, the error bars are smaller than the symbol size.

Comparison of the 10 K and room temperature Mössbauer spectra of these glasses based on Eq. (1), suggests a correction factor, C_{293}/C_{10}, of 1.105 ± 0.015 (2σ) (Fig. 2). Because recoilless fractions are not exactly unity even at 10 K, owing to the possibility of zero point effects on bond strengths (Chen and Yang, 2007), this correction represents a minimum value. We further examined the temperature dependence of recoilless fraction with a detailed study of Mössbauer spectra of glass AII_25 at 40–320 K.

With increasing temperature for glass AII_25, the relative area under the Fe^{2+} doublet diminishes compared to that of Fe^{3+} (Table S4), and the normalized area ratios decrease for both Fe^{3+} and Fe^{2+} (Fig. 3), as is also observed for andesitic glasses (Zhang et al., 2015). As the actual $Fe^{3+}/(Fe^{2+} + Fe^{3+})$ ratio of each sample, which is $N(Fe^{3+})/[N(Fe^{2+}) + N(Fe^{3+})]$, is the same in all cases, this temperature dependence is best understood as a relative change in recoilless fractions for Fe^{3+} and Fe^{2+}. This verifies that the uncorrected RT Mössbauer spectrum for AII_25 overestimates the true $Fe^{3+}/\Sigma Fe$ ratio. The temperature dependence to the absorption areas (*AA*) attributed to each ion can be approximated by a Debye function

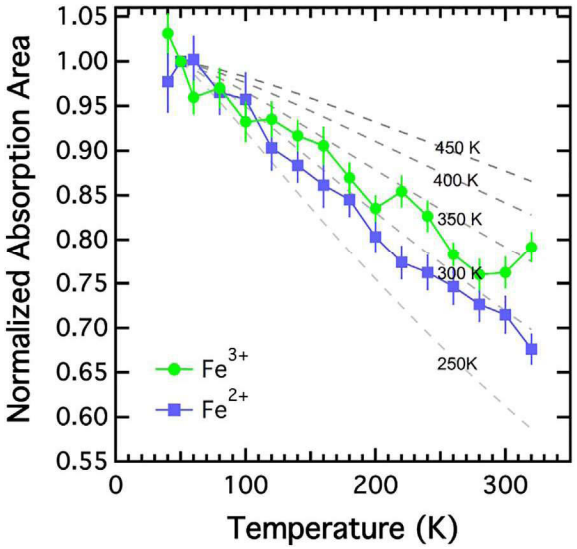

Fig. 3. Normalized absorption areas (*AA*) for Fe^{3+} and Fe^{2+} as a function of temperature from All_25 Mössbauer spectra fit with xVBF methods. The normalized areas are the absorption areas of Mössbauer paramagnetic doublets for Fe^{3+} and Fe^{2+} after the background has been removed, *AA*(T), divided by the absorption area of these doublets at a reference temperature, *AA*(T_0), which in this case is taken as T_0 at 50 K. Dashed curves are calculated normalized *AA*(T_0), where T_0 equals 50 K, from recoilless fractions calculated at different Debye temperatures.

$$\frac{AA(T)}{AA(T_0)} = \frac{f(T)}{f(T_0)} = \exp\left\{-\frac{6E_R}{k_B\theta_D}\left[\left(\frac{T}{\theta_D}\right)^2 \int_0^{\theta_D/T} \frac{x}{e^x-1}dx - \left(\frac{T_0}{\theta_D}\right)^2 \int_0^{\theta_D/T_0} \frac{x}{e^x-1}dx\right]\right\} \quad (3)$$

(De Grave et al., 1985; Chen and Yang, 2007; Zhang et al., 2015), where f is recoilless fraction, θ_D is the Mössbauer Debye temperature and the sole adjustable parameter in the equation, k_B is the Boltzmann constant, E_R is the recoil energy, which in turn is given by $E_R = E_g^2/2Mc^2$, in which E_g is the energy of the γ-rays (14.412 keV to excite ^{57}Fe), M is the mass of the absorber (^{57}Fe = 56.935 amu), and c is the velocity of light (c = 299,792,458 m/s).

Analysis of the recoilless fraction in this manner is termed the relative method (Chen and Yang, 2007; Zhang et al., 2015). Additionally, center shifts (CS) increase with decreasing temperature, consistent with the contributions of the second-order Doppler shift (Fig. S3), and this in turn can be related to differences in Mössbauer Debye temperatures of Fe^{3+} and Fe^{2+}, and therefore to differences in recoilless fraction (De Grave et al., 1985). As discussed by Zhang et al. (2015), the relative method is preferred because it is more direct and less reliant on the applicability of Debye theory, which does not account for possible contributions from anharmonicity that may be particularly important for glasses.

As described by Zhang et al. (2015), Mössbauer Debye temperatures can be determined by direct measurement of the temperature-dependent relative areas of the Mössbauer doublets (Eq. (2)), calculated by normalizing to measurements at a reference temperature (T_0). In theory, one should be able to use any temperature step as T_0 and get the same answer. However, using a single T_0 has the effect of exaggerating the weight of the uncertainty of Mössbauer spectra collected at the selected reference temperature relative to uncertainties on spectra collected at the other temperatures used to refine θ_D. To avoid this bias, we calculated θ_D repeatedly using the data collected from 40 to 320 K by selecting every measurement temperature as T_0 and resolving θ_D over the temperature range. We then calculate an averaged θ_D considering uncertainties from each θ_D determination. The individual values of θ_D for Fe^{2+} and Fe^{3+} for the basalts are listed in Table 1 and the average Mössbauer Debye temperatures for AII_25 are 339 ± 24 K and 292 ± 7 K, in 2σ for Fe^{3+} and Fe^{2+}, respectively. From these determinations of Mössbauer Debye temperatures, recoilless fractions can be calculated as a function of temperature (Chen and Yang, 2007; Zhang et al., 2015). At each T_0, the values of C_{293} in Eq. (1), calculated with θ_D^{T0}, are listed in Table 1 and the average value is 1.125 ± 0.068, in 2σ. This value agrees well with the estimate (C_{293} = 1.105 ± 0.015) derived from comparison of 10 K and 293 K analyses of the suite of basaltic glasses with a range of Fe^{3+}/Fe^{2+} ratios (Fig. 2). The agreement of these two independent approaches supports the accuracy of the derived C_{293} values. In the following calculations, we adopt the 1.125 ± 0.068 value for application to basaltic glasses because, as described earlier, it is likely to be more accurate.

Table 1
Debye T, θ_T, and correction number, C_T, (at 293 K) calculated from normalized area ratios (A(T)/A(T_0)) as a function of temperature for basalt glass AII_25.

T_0[a]	C[b]	θ_T (Fe^{3+})	θ_T (Fe^{2+})
40	1.019(49)	312(18)	305(2)
50	1.120(38)	330(15)	289(2)
60	1.209(43)	360(20)	283(1)
80	1.129(38)	337(16)	291(2)
100	1.206(58)	358(28)	283(2)
120	1.101(38)	337(16)	299(2)
140	1.114(23)	337(10)	295(1)
160	1.116(24)	335(10)	293(1)
180	1.118(20)	336(8)	293(1)
200	1.110(24)	326(9)	289(1)
220	1.190(33)	351(14)	284(2)
240	1.147(37)	343(16)	290(2)
260	1.069(38)	319(14)	294(1)
280	1.055(36)	315(13)	296(3)
300	1.077(40)	334(17)	304(3)
320	1.229(31)	386(18)	291(2)
Average	1.125(68)	339(24)	292(7)

Note: the uncertainty notation is such that, for example, 1.019(49) is equivalent to 1.019 ± 0.049. Uncertainties are given as 2σ standard deviations. The average value is calculated as the weighted mean of determinations at individual temperatures.
[a] T_0: temperature in K.
[b] $C = f(Fe^{3+})/f(Fe^{2+})$.

Zhang et al. (2015) calculated C_{293} for two andesitic glasses, one quenched at ambient pressure (VF3) and one quenched from high pressure (M544), using just one reference temperature. Therefore, we have recalculated the Mössbauer Debye temperatures and C_{293} for these glasses in Zhang et al. (2017) and provide here an updated andesite-specific XANES calibration in supplement Fig. S4 that we discuss in Section 4.1. The resulting average θ_D for Fe^{3+} and Fe^{2+} are 334 ± 25 K and 273 ± 16 K, in 2σ, respectively for VF3 and 361 ± 29 K and 303 ± 21 K, in 2σ, respectively for M544; and the values of C_{293} are 1.200 ± 0.111, in 2σ for VF3 and 1.138 ± 0.088, in 2σ for M544. These values are slightly lower, but within uncertainty, of those calculated from the relative method by Zhang et al. (2015) (1.256 ± 0.0153 and 1.151 ± 0.118, for VF3 and M544, respectively) using a single reference temperature instead of the calculated average from a range of reference temperatures, as calculated here.

4. Revised calibration for $Fe^{3+}/\Sigma Fe$ from XANES pre-edge centroids

4.1. Basalt and andesite

The correction factor, C_{293}, calculated here for basalt (1.125 ± 0.068), allows recalculation of the $Fe^{3+}/\Sigma Fe$ ratios of the 13 basaltic glasses employed as standards by Cottrell et al. (2009). The resulting revised $Fe^{3+}/\Sigma Fe$ ratios for these basalts are given in Table 2. The revised $Fe^{3+}/\Sigma Fe$ ratios of these standards, in turn, allow recalibration of the relationship between the XANES pre-edge centroid

Table 2
Updated drift corrected centroid energies and $Fe^{3+}/\Sigma Fe$ for standard basaltic glasses, using averaged data collected at NSLS over 8 years.

Sample name	Cottrell et al. (2009)	n[a]	This work	$Fe^{3+}/\Sigma Fe$[b]
LW_-20	7112.112(0.003)	48	7112.112(0.010)	0.079(0.006)
AII_-15	7112.144(0.010)	30	7112.147(0.026)	0.084(0.005)
LW_-10	7112.156(0.002)	45	7112.154(0.024)	0.117(0.005)
AII_-05	7112.217(0.011)	33	7112.219(0.010)	0.125(0.004)
AII_0	7112.279(0.006)	33	7112.275(0.010)	0.133(0.004)
LW_0	7112.299(0.002)	24	7112.300(0.010)	0.147(0.003)
AII_05	7112.355(0.011)	39	7112.361(0.011)	0.176(0.004)
LW_10	7112.439(0.002)	48	7112.434(0.013)	0.214(0.004)
AII_15	7112.511(0.009)	39	7112.520(0.013)	0.226(0.004)
LW_20	7112.611(0.008)	39	7112.608(0.020)	0.279(0.005)
AII_25	7112.740(0.009)	30	7112.742(0.014)	0.329(0.005)
AII_35	7112.937(0.014)	30	7112.962(0.027)	0.455(0.004)
AII_45	7113.163(0.019)	33	7113.184(0.025)	0.583(0.005)

Note: all uncertainties here are 1σ standard deviations (1σ).
[a] n is number of analyses used to construct average.
[b] $Fe^{3+}/\Sigma Fe$ ratios are determined by Mössbauer spectroscopy from Cottrell et al. (2009), corrected for recoilless fraction effects using $C_{293} = 1.125$, as described in text, with the uncertainties reflecting only the statistics of the fits to the spectra.

position and the $Fe^{3+}/\Sigma Fe$ ratio. We use the same method for determining drift-corrected pre-edge centroid positions described in Cottrell et al. (2009), but with updated measurements of the centroids for the standards that reflect improved statistics from > 8 years of repeated measurements of these glasses at beamline X26A of National Synchrotron Light Source (NSLS). Revised centroid energies for each are given in Table 2.

Combining the revised $Fe^{3+}/\Sigma Fe$ ratios and pre-edge centroids for the 13 basalt standards allows regression of a modified XANES calibration curve that can be applied to determine $Fe^{3+}/\Sigma Fe$ ratios in unknown basaltic glasses (Fig. 4). We applied a weighted least-squares, second-order polynomial fit to the reference glasses, taking into account the uncertainties in precision of the XANES and Mössbauer data in Table 2. The new calibration is applicable for basalts with $Fe^{3+}/\Sigma Fe$ ratios between 0.08 and 0.6, has a R^2 of 0.996, and is given by

$$y = \frac{Fe^{3+}}{\Sigma Fe} = a_1 + a_2 x + a_3 x^2 \quad (4)$$

where x is the drift-corrected centroid energy minus 7112.22 eV, $a_1 = 0.011$, $a_2 = 0.354$, and $a_3 = 0.125$ (Table 3 and Table S5).

The quantitative uncertainties for calculating $Fe^{3+}/\Sigma Fe$ ratios from the XANES calibration depicted in Fig. 4 depend on the relevant comparison. For comparison of $Fe^{3+}/\Sigma Fe$ ratios determined by XANES, the precision of the analyses depends only on the instrumental uncertainty associated with the centroid determination, σ_x. The uncertainty in $Fe^{3+}/\Sigma Fe$ ratio that arises from σ_x is here termed σ_{y1}, which is given by

$$\sigma_{y1} = \sqrt{(a_2 + 2a_3 x)^2 {\sigma_x}^2}. \quad (5)$$

Comparison of $Fe^{3+}/\Sigma Fe$ ratios determined by XANES to $Fe^{3+}/\Sigma Fe$ ratios determined by Mössbauer spectroscopy requires consideration of the uncertainties associated with the coefficients (a_1, a_2, and a_3) to the quadratic function given in Eq. (4), determined by the least squares methods described above, in addition to instrumental uncertainties of the XANES determinations. We term this uncertainty σ_{y2}. Importantly, the coefficients resulting from the least squares fit have covariances as well as variances, and are described by the variance-covariance matrix (Bevington and Robinson, 2003)

$$cov = \begin{vmatrix} \sigma_{a1}^2 & \sigma_{a1a2}^2 & \sigma_{a1a3}^2 \\ \sigma_{a2a1}^2 & \sigma_{a2}^2 & \sigma_{a2a3}^2 \\ \sigma_{a3a1}^2 & \sigma_{a3a2}^2 & \sigma_{a3}^2 \end{vmatrix}. \quad (6)$$

The numerical values of the elements of *cov* are given in Table S5, and σ_{y2} is given by

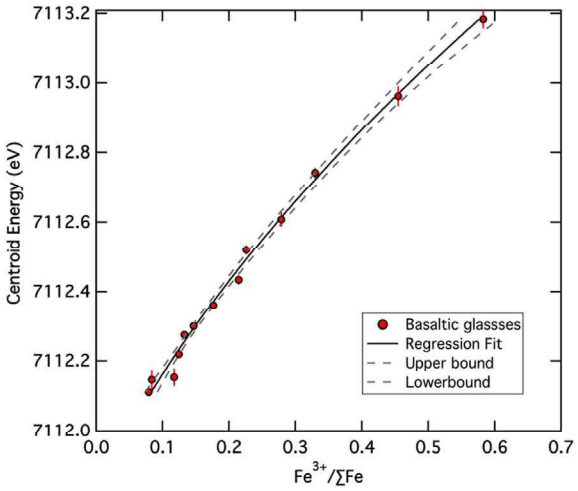

Fig. 4. Updated XANES calibration curve for determining $Fe^{3+}/\Sigma Fe$ ratios of basaltic glasses following Cottrell et al. (2009). The updated centroid energy values and $Fe^{3+}/\Sigma Fe$ ratios determined by Mössbauer spectroscopy and corrected for the effects of recoilless fraction are from Table 2, labeled as solid red circles. The solid curve is the weighted second-order polynomial fit result with dashed lines showing the 95% confidence band. The error bars are 1 σ standard deviation as listed in Table 2; in the x-axis direction, the error bars are smaller than the symbols. (For interpretation of the references to colour in this figure legend, the reader is referred to the web version of this article.)

Table 3
Regression coefficients from weighted least-square fits and R^2 of those fits.

	μ	a_1	a_2	a_3	R^2
Basaltic	7112.22	0.11956	0.35377	0.12450	0.996
Andesitic	7113.25	0.64116	0.77511	0.26251	0.992
Mafic	7112.22	0.11560	0.24066	0.28538	0.991

Note: uncertainties are listed in Table S4.
$y = a_1 + a_2(x - \mu) + a_3(x - \mu)^2$, where y refers $Fe^{3+}/\Sigma Fe$ ratio and x refers centroid from pre-edge XANES spectra. = as number of analyses used to construct average.

$$\sigma_{y2} = \sqrt{X^T\, cov\, X + \sigma_{y1}^2}, \quad (7)$$

where X is the vector

$$\begin{vmatrix} 1 \\ x \\ x^2 \end{vmatrix}. \quad (8)$$

Finally, for comparison of XANES-determined values of $Fe^{3+}/\Sigma Fe$ ratios to $Fe^{3+}/\Sigma Fe$ ratios determined by independent methods such as wet chemistry, we must also consider the contributions to uncertainty arising from the statistically imperfect resolution of the value of the recoilless fraction ratio, C_{293}. These are systematic uncertainties, in that adopting different values of C_{293} would result in shifts of all the calibration points in Fig. 4 to greater or lesser values of $Fe^{3+}/\Sigma Fe$ ratios, and incorporation of this effect is an evaluation of the accuracy (rather than simply the precision) of the $Fe^{3+}/\Sigma Fe$ ratio determined by the XANES calibration. This accuracy uncertainty is termed σ_{y3} and from propagation of uncertainty through Eq. (2) is given by

$$\sigma_{y3} = \sqrt{\left(\frac{C_{293}}{[y + C_{293}(1-y)]}\right)^2 \sigma_y^2 + \left(\frac{y(y-1)}{[y + C_{293}(1-y)]}\right)^2 \sigma_{C_{293}}^2} \quad (9)$$

As Eq. (9) is derived from Eq. (2), the values of y and σ_y that are strictly applicable are for the apparent $Fe^{3+}/\Sigma Fe$ ratio determined from room temperature Mössbauer analyses, y_{293}. But because such values of y correlate strongly with other values, such as those determined by temperature-corrected Mössbauer analysis or XANES, Eq. (9) can be used to incorporate the accuracy uncertainty deriving from imperfectly constrained values of C_{293} for other determinations of $Fe^{3+}/\Sigma Fe$ ratio

for which precision is characterized.

The same procedures can be applied to a revised calibration of Mössbauer-determined $Fe^{3+}/\Sigma Fe$ ratios for the 19 andesitic glasses analyzed by Zhang et al. (2016), using the applicable correction factor, C_{293}, of 1.200 ± 0.111 (Table S7 in Zhang et al., 2017). For these, the fit parameters to Eq. (4) are $a_1 = 0.641$, $a_2 = 0.775$, and $a_3 = 0.263$, where x is the drift-corrected centroid energy minus 7113.25 eV (Table 3 and Table S5). This fit has a R^2 of 0.992 and is applicable for values of $Fe^{3+}/\Sigma Fe$ between 0.08 and 0.80. Uncertainties can be calculated from the covariance matrix (Eq. (6)) given in Table S5. The resulting relationship between $Fe^{3+}/\Sigma Fe$ and XANES centroids is shown in Fig. S4.

The statistics cited above indicate how well the regressions recover the Mössbauer-determined $Fe^{3+}/\Sigma Fe$ ratios of the calibration glass standards, but do not necessarily predict the uncertainties that can be attached to newly analyzed unknowns. Some insight for such predictive capacity can be attained from cross-validation methods. Because the data sets used to train the model are small ($n_{basalt} = 13$ and $n_{andesite} = 19$), we use the leave-one-out cross-validation method (Arlot and Celisse, 2010) to run this test. The resulting root mean square uncertainties for the predicted $Fe^{3+}/\Sigma Fe$ ratios of unknowns determined from the basaltic and andesitic calibrations are, respectively, ± 0.01 (1σ) and ± 0.02 (1σ).

4.2. General calibration for mafic glasses

The revised $Fe^{3+}/\Sigma Fe$ ratio calculations for basaltic and andesitic glasses also allow presentation of a more general XANES calibration for mafic glasses when compositions are intermediate between basalt and andesite and/or when the available calibration glasses are not an exact match to the unknowns. Dauphas et al. (2014) and Zhang et al. (2016) previously showed that the XANES Fe pre-edge centroids of basaltic and andesitic glasses have similar correspondences to their $Fe^{3+}/\Sigma Fe$ ratios. Going further, Dyar et al. (2016) highlighted the versatility of applying a single universal calibration to silicate glasses from basalt to rhyolite in cases where 3.6% (1 σ) absolute precision on the $Fe^{3+}/\Sigma Fe$ ratio is acceptable. Here, we develop a function that may be applied to mafic glasses (basalt through andesite) using the 13 basaltic glass standards from Cottrell et al. (2009) and the 19 andesitic glasses from Zhang et al. (2016), corrected for recoilless fraction based on the results of this work and of Zhang et al. (2017), in addition to 6 iron-rich synthetic basaltic glasses analyzed for $Fe^{3+}/\Sigma Fe$ ratio by wet chemistry (Kress and Carmichael, 1991) and by XANES (Cottrell and Kelley, 2011). Together, these glasses range in SiO_2 from 45 to 57 wt% SiO_2. The qualitatively distinct nature of uncertainties in Mössbauer and wet chemical analyses makes Monte Carlo simulation the optimum method for evaluating the best fit curve and its attendant propagated confidence interval, as detailed in the caption to Fig. 5. The resulting best fit with $R^2 = 0.991$ is described by Eq. (4) with the coefficients $a_1 = 0.1156$, $a_2 = 0.2407$, and $a_3 = 0.2854$ (Table 3 and Table S5) and is illustrated in Fig. 5. Uncertainties for σ_{y2} for this polynomial are described by Eq. (8), with coefficients of the covariance matrix given in Table S5. Note that there is no need to evaluate σ_{y3} in this case because the uncertainties in the values of the recoilless fraction are already factored into the Monte Carlo simulation. The expected uncertainty in $Fe^{3+}/\Sigma Fe$ ratio of an analyzed unknown using the mafic glass calibration, estimated with the leave-one-out cross validation method described above, is ± 0.02 (1σ).

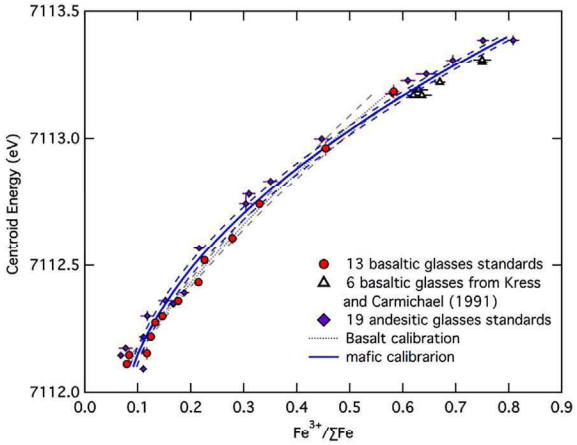

Fig. 5. XANES calibration curve for determining $Fe^{3+}/\Sigma Fe$ ratios of mafic glasses with SiO_2 ranging from 45 wt% to 57 wt%. Updated centroid energy values and corrected $Fe^{3+}/\Sigma Fe$ ratios for basaltic (solid red circles) and andesitic (solid purple diamonds) glasses analyzed originally by Cottrell et al. (2009) and Zhang et al. (2016) corrected $Fe^{3+}/\Sigma Fe$ ratios are described in the text and given in Table 2 and Table S5, respectively. For 3 andesitic glasses analyzed by Zhang et al. (2016) both at NSLS and APS facilities, centroids and uncertainties are averages. XANES centroids are given in Cottrell and Kelley (2011) for 6 basaltic glasses (empty black triangles) analyzed by wet chemistry by Kress and Carmichael (1991). The heavy, solid blue line is the weighted second-order polynomial fit with blue dashed lines showing the 95% confidence band. For reference, the gray dotted and dashed lines show the basaltic XANES calibration curve and 95% confidence band given by Eq. (4) and shown in Fig. 4. Error bars have the same format as in Fig. 4. (For interpretation of the references to colour in this figure legend, the reader is referred to the web version of this article.)

5. Discussion

5.1. Mössbauer recoilless fraction ratio in mafic glasses

The improved and recommended recoilless fraction ratios at room temperature, C_{293}, for basaltic and andesitic glasses are 1.125 ± 0.068 and 1.200 ± 0.111, respectively. Although these are similar within uncertainty, a larger value for andesitic than for basaltic glass could indicate that the difference in Fe^{3+}–O and Fe^{2+}–O bond strengths in the andesitic glass is greater than that for basaltic glass. The recoilless fractions of Fe^{3+} and Fe^{2+} found for mafic glasses are comparable to those expected based on measurements of f_{293} in minerals (Leider and Pipkorn, 1968; Seifert and Olesch, 1977; Chambaere et al., 1984; De Grave et al., 1984; De Grave et al., 1985; Vandenberghe et al., 1986; Bowen et al., 1989; Ellwood et al., 1989; Persoons, 1990; De Grave and Van Alboom, 1991; de Bakker, 1994; Fei et al., 1994; McCammon et al., 1995; Van Alboom and De Grave, 1996; De Grave et al., 1998; McCammon, 1998; Eeckhout et al., 1999; Eeckhout et al., 2000; Eeckhout and De Grave, 2003; Dyar et al., 2008; Dyar et al., 2012; Dyar et al., 2013) (Fig. 1) and glasses (Ottonello et al., 2001; Mysen and Dubinsky, 2004; Mysen, 2006).

5.2. Accuracy of basalt glass $Fe^{3+}/\Sigma Fe$ ratios determined by Mössbauer spectroscopy

Berry et al. (2015, 2017) suggested that the $Fe^{3+}/\Sigma Fe$ ratios determined for MORB by Cottrell and Kelley (2011) are greater than wet-chemical determinations by Christie et al. (1986) and Bézos and Humler (2005) owing to inappropriate interpretation of the Mössbauer spectra of the 13 glasses used as standards by Cottrell et al. (2009). The basis for this assertion is an alternate interpretation of an asymmetry, a "shoulder," on the low-velocity side of the high-velocity component of the Mössbauer absorption doublet in glasses equilibrated at oxygen fugacities below QFM. A feature found in the spectra of tektites with similar hyperfine parameters (CS near 0.6 mm/s and QS near 1 mm/s) was called "D2" by Rossano et al. (1999). Following Rossano et al. (1999), Berry et al. (2015, 2017) argued that "D2" must derive from Fe^{2+} because it occurs in highly reduced glasses, and conjectured that it could also be present in the Mössbauer spectra of the more oxidized glasses used for XANES calibration by Cottrell et al. (2009), thereby biasing the latter's calibration to higher $Fe^{3+}/\Sigma Fe$ ratios.

Features similar to "D2", but with somewhat distinct hyperfine features, have been identified in reduced glasses by Virgo and Mysen (1985) (at 77 K) and by Borisov and McCammon (2010). Cottrell et al.

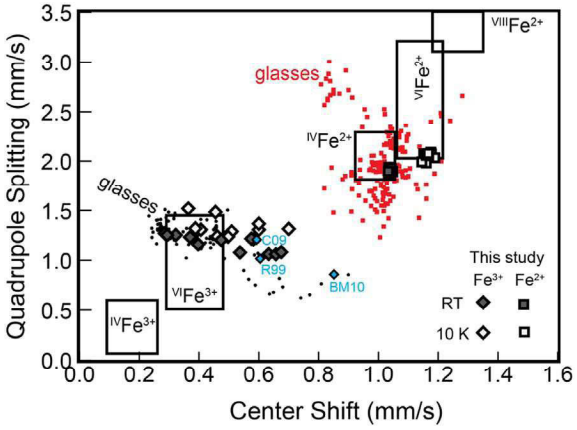

Fig. 6. Survey of room temperature and 10 K Mössbauer hyperfine parameters for paramagnetic Fe^{2+} and Fe^{3+} from glasses and minerals. Parameters for glasses, shown as black circles (Fe^{3+}) and red squares (Fe^{2+}), come from Mysen et al. (1985); Jayasuriya et al. (2004); Rossano et al. (2008); Borisov and McCammon (2010); Zhang et al. (2016), and shown as diamonds (Fe^{3+}) and squares (Fe^{2+}) for Cottrell et al. (2009) with room temperature (dark gray symbols) and 10 K (empty symbols) Mössbauer hyperfine parameters given in Table S2 and Table S3 of this study, respectively. Black boxes outline fields for minerals with Fe^{2+} and Fe^{3+} in different coordination states, after Dyar et al. (2006). The small "D2" feature evident in the three most reduced glasses from Cottrell et al. (2009) (C09) and Rossano et al. (1999) (R99) has parameters similar to Fe^{3+} in glasses and not greatly different for Fe^{3+} in minerals, but is distinct from the expression of Fe^{2+} in glasses or minerals (blue diamonds). The feature observed in reduced glasses by Borisov and McCammon (2010) (BM10; a blue diamond) has a greater Center Shift and its origin may not be the same as the "D2" feature. Dyar et al. (2006) also include a large field for Fe^{2+}-Fe^{3+} electron delocalization that plots close to the "D2" parameters. However, the dimensions of this field are not well constrained by observations and we are aware of no charge-delocalization features with room temperature hyperfine parameters similar to "D2". For example, for ilvaite, Fe^{2+}–Fe^{3+} charge delocalization has CS = 0.8–0.9 and QS = 1.6–1.9 (Dyar et al., 2006). (For interpretation of the references to colour in this figure legend, the reader is referred to the web version of this article.)

(2009) discussed this feature and considered it to be possibly owing to Fe^{3+} but, like Borisov and McCammon (2010), argued that it was not a statistically resolvable feature. Here we offer further analysis of this feature. In the following paragraphs, we show that (1) this feature (CS near 0.6 mm/s and QS near 1 mm/s) is most consistent with ferric iron, (2) the CS of ferric iron shifts to lower values as $Fe^{3+}/\Sigma Fe$ ratio increases (Virgo and Mysen, 1985; Dingwell and Virgo, 1987; Jayasuriya et al., 2004; Mysen, 2006; Zhang et al., 2016), and (3) attempts to retain a doublet with the hyperfine parameters of "D2" when fitting spectra of more oxidized glasses results in no statistical improvement or difference in the quality of the fit.

Rossano et al. (1999), analyzing tektites by wet chemistry, determined that 5–9% of iron in the tektites was ferric. Rossano et al. (1999) asserted, however, that because tektites are "known to be highly reduced", the absorption doublet, "D2" (CS ~0.6, QS ~1.0) must be attributable to a second ferrous site. Critically, however, the hyperfine features of "D2" are not close to any features known to be associated with Fe^{2+} in minerals or glasses, but are similar to those attributable to Fe^{3+} (Burns, 1994). Fig. 6 compares the hyperfine parameters of "D2" evident from the glasses of Rossano et al. (1999), Cottrell et al. (2009), this study, and a survey of Fe^{2+} and Fe^{3+} in glasses with those of Fe^{2+} and Fe^{3+} in a variety of coordination states in minerals from the compilation of Dyar et al. (2006). "D2" hyperfine parameters are close to those typical of Fe^{3+} and highly dissimilar to those of Fe^{2+} in silicate glasses and minerals. This comparison indicates that the "D2" feature arises from Fe^{3+}.

Fig. 6 reveals a broad range of mean CS values for Fe^{3+} in glasses measured in this study and reported in the literature. It is well established that the center shift of ferric iron varies with composition and oxidation state, typically decreasing as $Fe^{3+}/\Sigma Fe$ ratio increases (Virgo and Mysen, 1985; Dingwell and Virgo, 1987; Jayasuriya et al., 2004; Mysen, 2006; Zhang et al., 2016), consistent with a change in the structural role of ferric iron (Kress and Carmichael, 1988). While Fe^{3+} in every glass has a distribution of oxygen coordination numbers, in relatively reduced glasses in this and other studies, the most probable value of the CS of ferric iron is relatively high and similar to the hyperfine parameters of Rossano's "D2" (e.g. LW_-10, Fig. S5a). In more oxidized glasses, the most probable CS of ferric iron is lower (e.g. Table S2, AII_25, Fig. S2a). Our attempt to retain a third doublet with hyperfine parameters akin to "D2" (AII_25, Fig. S5b) resulted in a fit statistically indistinguishable from one without inclusion of the "D2" doublet within > 99% confidence (F-test statistic = 1.0000, p-value = 0.9999, degrees of freedom = 255). Inclusion of a second ferrous doublet is thus not justified by the statistics of the fits.

With respect to the intercalibration of XANES and Mössbauer determinations of $Fe^{3+}/\Sigma Fe$ ratios, we emphasize that, like Cottrell et al. (2009), we do not include glasses equilibrated below QFM-2.5. This stems from a structural interference that inhibits our ability to resolve changes in the pre-edge centroid for glasses with $Fe^{3+}/\Sigma Fe$ ratios < ~0.08 (Cottrell and Kelley, 2011). Thus, for the purpose of calibrating XANES, our fits of Mössbauer spectra taken on glasses equilibrated below QFM-2.5 is of little consequence because, as shown above, it does not impact our fits of glasses equilibrated above QFM-2.5.

5.3. Comparison to thermodynamic models

Because the 13 basaltic glasses used as standards in this study were quenched from 1350 °C and 100 kPa at known fO_2 (Cottrell et al., 2009), the $Fe^{3+}/\Sigma Fe$ ratios inferred from XANES centroids can be compared to those predicted from the thermodynamic models of Kress and Carmichael (1991) (their Eq. (7)) and Jayasuriya et al. (2004) (their Eq. (14)). Because the Kress and Carmichael (1991) model was calibrated from glasses analyzed by micro-colorimetry, this comparison tests the agreement between the XANES calibration and wet chemical determinations of $Fe^{3+}/\Sigma Fe$ ratio. Cottrell et al. (2009) found that their XANES calibration, based on uncorrected RT Mössbauer spectra, resulted in $Fe^{3+}/\Sigma Fe$ ratios slightly greater than those calculated from the Kress and Carmichael (1991) model, with an average offset in $Fe^{3+}/\Sigma Fe$ ratio of 0.017. Cottrell and Kelley (2011) applied micro-colorimetry, the same wet chemical method used to calibrate the model of Kress and Carmichael (1991), to some of their experimental glasses and concluded that the RT Mössbauer-based XANES calibration of Cottrell et al. (2009) might overestimate the ferric iron content of basalts by about 1% (absolute).

We find that the agreement improves between $Fe^{3+}/\Sigma Fe$ ratios calculated from XANES in this study (Eq. (4)) and $Fe^{3+}/\Sigma Fe$ ratios calculated from the thermodynamic model of Kress and Carmichael (1991) when treating the basaltic standards as unknowns. The comparative regression yields a slope of 1.000 and an average difference of 0.004 (Fig. 7). The improved agreement between the revised XANES calibration and the wet-chemically-derived model of Kress and Carmichael (1991) aids confidence in the accuracy of this study's XANES calibration.

The thermodynamic model of Jayasuriya et al. (2004) addresses the lack of any term in Sack et al. (1980) (a predecessor to Kress and Carmichael (1991)) that describes Fe^{2+}–Fe^{3+} interactions. Jayasuriya et al. (2004) compare their theoretical model to RT Mössbauer spectroscopic measurements of anorthite-diopside eutectic glasses containing 1 wt% Fe_2O_3. The spectroscopic approach postulates many different Fe^{2+} environments modeled by multiple symmetric Lorentzian doublets with equal widths. While thermodynamically satisfying, the Jayasuriya et al. (2004) model predicts the $Fe^{3+}/\Sigma Fe$ ratios measured in this study less accurately, given the basalt glass compositions and experimental furnace conditions. Regression of the $Fe^{3+}/\Sigma Fe$ ratios predicted by Jayasuriya et al. (2004) against measured $Fe^{3+}/\Sigma Fe$ ratios from Cottrell et al. (2009) and this work yields a slope of 0.872 and 0.780, respectively, and an average difference of 0.045

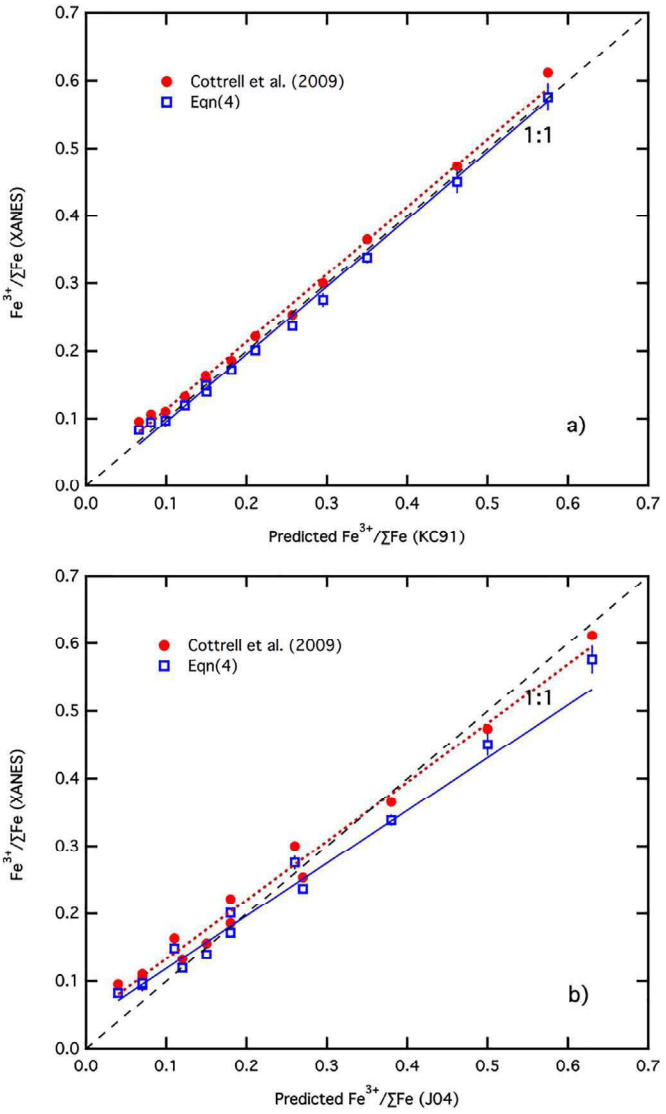

Fig. 7. Comparison of $Fe^{3+}/\Sigma Fe$ ratios in the 13 standard glasses from Cottrell et al. (2009) determined by Mössbauer-based XANES relative to ratios predicted by the thermodynamic model of a) Kress and Carmichael (1991) and b) Jayasuriya et al. (2004) based on melt composition, temperature and fO_2 from which the glasses were quenched. The Kress and Carmichael (1991) model is calibrated from micro-colorimetric wet chemical determinations of $Fe^{3+}/\Sigma Fe$ ratios. The Jayasuriya et al. (2004) model is calibrated from room temperature Mössbauer determinations of $Fe^{3+}/\Sigma Fe$ ratios. The dashed black line shows 1:1 correspondence. The solid red circles and the empty blue squares are $Fe^{3+}/\Sigma Fe$ ratios calculated from the XANES calibrations of Cottrell et al. (2009) and Eq. (4) in this work, respectively. The red dotted and blue sold lines are linear regressions incorporating uncertainties in $Fe^{3+}/\Sigma Fe$ ratios from the XANES calibrations, a) resulting in the relations C09 = 1 * KC91 + 0.014, R^2 = 0.995 and EQ4 = 1 * KC91–0.005, R^2 = 0.995, respectively, and b) resulting in the relations C09 = 0.872 * J04 + 0.045, R^2 = 0.986 and EQ4 = 0.780 * J04 + 0.041, R^2 = 0.849, respectively, where C09, and EQ4 are, respectively, the $Fe^{3+}/\Sigma Fe$ ratios from the XANES calibrations of Cottrell et al. (2009) and Eq. (4) of this work, and KC91 and J04 are the $Fe^{3+}/\Sigma Fe$ ratios predicted by Kress and Carmichael (1991) and Jayasuriya et al. (2004), respectively. All the calculated $Fe^{3+}/\Sigma Fe$ ratios are listed in Table S6. (For interpretation of the references to colour in this figure legend, the reader is referred to the web version of this article.)

and 0.041, respectively (Fig. 7).

5.4. Revised estimates of MORB glass $Fe^{3+}/\Sigma Fe$ ratios

The revised XANES calibration allows an updated estimate of the $Fe^{3+}/\Sigma Fe$ ratios of natural glasses analyzed by XANES. Of particular importance is a re-evaluation of the $Fe^{3+}/\Sigma Fe$ ratios of mid-ocean ridge basalts (MORB), which relate directly to the fO_2 conditions of the modern oceanic upper mantle. Applying Eq. (4) to the 103 MORB glasses analyzed by Cottrell and Kelley (2011) (Table S7) yields an average $Fe^{3+}/\Sigma Fe$ ratio of 0.143 ± 0.008, where the uncertainty reflects only XANES precision (σ_{y1}). This value is modestly smaller than the ratio of 0.16 ± 0.01 reported by Cottrell and Kelley (2011) that arises from the uncorrected calibration of Cottrell et al. (2009). Although not the topic of focus in this work, other determinations of $Fe^{3+}/\Sigma Fe$ ratios in basaltic glasses that have employed the Cottrell et al. (2009) calibration will also decrease by a similar amount, based on the revised calibration of Eq. (4).

To compare average MORB $Fe^{3+}/\Sigma Fe$ ratios determined by XANES with averages determined from wet chemistry, such as those of Christie et al. (1986) or Bézos and Humler (2005), requires incorporation of the effects of systematic error arising from uncertainties in the recoilless fraction. The magnitude of this systematic uncertainty can be approximated by Eq. (9). Because the absolute values of the $Fe^{3+}/\Sigma Fe$ ratio in MORB are relatively low, this effect is small, raising the 1σ uncertainty from 0.008 to 0.01. Thus, including uncertainties associated with accuracy as well as precision, the $Fe^{3+}/\Sigma Fe$ ratio of average MORB determined by XANES is 0.14 ± 0.01 (1σ).

This downward adjustment in MORB $Fe^{3+}/\Sigma Fe$ ratio compared to that of Cottrell and Kelley (2011) brings the average $Fe^{3+}/\Sigma Fe$ ratio of MORB measured by XANES closer to the average ratios measured by wet chemistry of 0.12 ± 0.02 (1σ) by Bézos and Humler (2005) and 0.07 ± 0.03 (1σ) by Christie et al. (1986). An analysis of the standard errors, however, reveals that the mean oxidation state of iron in MORB found in this study, 0.143 ± 0.001 (1SE, n = 103), remains significantly higher (*t*-test statistic 8.56, p-value = 2.6e15) than, for example, the mean of 0.124 ± 0.002 (1SE, n = 105) determined by Bézos and Humler (2005).

Ottonello et al. (2001) and Lange and Carmichael (1989) raised the possibility that Mössbauer yields systematically higher $Fe^{3+}/\Sigma Fe$ ratios for glasses than wet chemistry due to recoilless fraction effects. Consistent with these suggestions, we show here that, with a correction for recoilless fraction, no bias exists for the experimental calibration glasses between our Mössbauer-derived $Fe^{3+}/\Sigma Fe$ ratios and those predicted from the algorithm of Kress and Carmichael (1991), which is based on the same wet chemical technique as the Christie et al. (1986) study (Fig. 7). Moreover, the fO_2 we calculate from XANES-based basalt $Fe^{3+}/\Sigma Fe$ ratios agrees with spinel oxybarometry performed on the same experiments (Davis and Cottrell, in revision).

Similar to the conclusions of Cottrell and Kelley (2011), we suggest that the apparent bias between Mössbauer (or Mössbauer-calibrated XANES) and wet-chemistry is most evident when analyses of natural samples are considered. Cottrell and Kelley (2011) and Bézos and Humler (2005) discuss how incorporation of micro-phenocrysts in bulk wet chemical analyses or the influence of additional redox couples present in natural samples, such those owing to sulfur, could lead wet-chemically derived $Fe^{3+}/\Sigma Fe$ ratios of natural samples, but not synthetic samples, to diverge from XANES-derived $Fe^{3+}/\Sigma Fe$ ratios. Alternatively, if the mantle is heterogeneous on a segment or basin scale, the analyzed samples in each study may be biased towards populations that do not have similar mean redox states. For example, the basalts analyzed by Bézos and Humler (2005) come dominantly from the Indian Ocean (58 out of 105 samples), which may be more reduced than other ocean basins (Cottrell and Kelley, 2013; Kelley and Cottrell, 2016). Discrimination among these possibilities awaits further study.

5.5. Oxygen fugacity in the MORB-source mantle

The oxygen fugacity (fO_2) of primitive MORB melts and of their source can be inferred from the $Fe^{3+}/\Sigma Fe$ ratios of MORB glasses (Carmichael and Ghiorso, 1986; Ballhaus, 1993; Frost and McCammon, 2008; Cottrell and Kelley, 2011). Based on an average MORB $Fe^{3+}/\Sigma Fe$ ratio of 0.16 ± 0.01, Cottrell and Kelley (2011) inferred a mean fO_2 of 0.10 ± 0.18 log units above the QFM buffer of Frost (1991) by

applying the Kress and Carmichael (1991) model at 1200 °C and 100 kPa. The revised mean MORB $Fe^{3+}/\Sigma Fe$ of 0.143 ± 0.008 determined here results in conditions about 0.25 log units more reduced, with a mean value of QFM-0.18 ± 0.16.

6. Conclusions

We reevaluated the XANES calibration to determine $Fe^{3+}/\Sigma Fe$ ratios of 13 basaltic standard glasses from Cottrell et al., 2009. These glasses were previously analyzed by RT Mössbauer spectroscopy, and in this paper, we took into account the effect of recoilless fraction on the apparent $Fe^{3+}/\Sigma Fe$ ratios measured from room temperature Mössbauer spectra. $f(Fe^{2+})$ and $f(Fe^{3+})$ in basaltic glass were calculated from variable-temperature Mössbauer spectra of AII_25 by a relative method (RM), which is based on the temperature dependence of the absorption area ratios of Fe^{3+} and Fe^{2+}. The correction value applicable to room temperature determinations (C_{293}) is 1.125 ± 0.068 (2σ). Applying the correction value to the $Fe^{3+}/\Sigma Fe$ ratios resolved from RT Mössbauer spectra and the revised average XANES pre-edge centroids for the 13 standard glasses allows regression of a new XANES basalt calibration. The XANES calibration for andesites (Zhang et al., 2016) is also updated and a more general XANES calibration for mafic glasses including both basaltic and andesitic compositions is provided in this work. With the updated basaltic XANES calibration, we have recaluculated $Fe^{3+}/\Sigma Fe$ ratios for the mid-ocean ridge basalt (MORB) glasses analyzed previously by XANES by Cottrell and Kelley (2011). Our results yield an average $Fe^{3+}/\Sigma Fe$ ratio for MORB of 0.143 ± 0.008 (1σ) taking into account only analytical precision, and 0.14 ± 0.01(1σ), taking into account uncertainty on the value of C_{293}. Based on the database of Cottrell and Kelley (2011), the revised average oxygen fugacity for MORB is $\Delta QFM = -0.18 \pm 0.16$, where the QFM buffer is calculated based on Frost (1991) at 100 kPa.

Supplementary data to this article can be found online at https://doi.org/10.1016/j.chemgeo.2018.01.006.

Acknowledgements

E.C. thanks Bjorn Mysen for generously sharing his Mössbauer facility, and his expertise. We are thankful for the thoughtful and thorough comments of two anonymous referees. M.H gratefully acknowledges support from NASA (NNX11AG64G) and NSF (EAR1426772). H.Z. acknowledges support from National Natural Science Foundation of China (41603058). E.C. acknowledges support from NSF OCE 1433212. K.K. acknowledges support from NSF OCE 1433182 and EAR 1347330. The Mössbauer temperature series was performed at the Institute for Rock Magnetism (IRM) at the University of Minnesota. The IRM is a US National Multi-user Facility supported through the Instrumentation and Facilities program of the National Science Foundation, Earth Sciences Division, and by funding from the University of Minnesota. We thank Tony Lanzirotti and Matt Newville for assistance during XANES data collection. XANES spectra were collected at Beamline X26A, National Synchrotron Light Source (NSLS), Brookhaven National Laboratory. X26A was supported by the Department of Energy (DOE) – Geosciences (DE-FG02-92ER14244 to The University of Chicago – CARS). Use of the NSLS was supported by DOE Office of Science under Contract No. DE-AC02-98CH10886. Portions of this work were also performed at GeoSoilEnviroCARS (The University of Chicago, Sector 13), Advanced Photon Source (APS), Argonne National Laboratory. GeoSoilEnviroCARS is supported by the National Science Foundation - Earth Sciences (EAR - 1634415) and Department of Energy- GeoSciences (DE-FG02-94ER14466). Use of the Advanced Photon Source was supported by the DOE Office of Science by Argonne National Laboratory under Contract No. DE-AC02-06CH11357.

References

Alberto, H.V., Pinto da Cunha, J.L., Mysen, B.O., Gil, J.M., Ayres de Campos, N., 1996. Analysis of Mössbauer spectra of silicate glasses using a two-dimensional Gaussian distribution of hyperfine parameters. J. Non-Cryst. Solids 194, 48–57.

Alderman, O., Wilding, M., Tamalonis, A., Sendelbach, S., Heald, S., Benmore, C., Johnson, C., Johnson, J., Hah, H.-Y., Weber, J., 2017. Iron K-edge X-ray absorption near-edge structure spectroscopy of aerodynamically levitated silicate melts and glasses. Chem. Geol. 453, 169–185.

Arlot, S., Celisse, A., 2010. A survey of cross-validation procedures for model selection. Statist. Surv. 4, 40–79.

de Bakker, P., 1994. Grondige Mossbauerstudie van de selectief magnetisch verdunde spinelsystemen $MgFe_{2-x}Cr_xO_4$ ($0.0 \le x \le 2.0$) en $Mg_{1-x}Zn_xFe_{1.5}Cr_{0.5}O_4$ ($0.0 \le x \le 1.0$) (PhD Thesis). Ghent University.

Ballhaus, C., 1993. Redox states of lithospheric and asthenospheric upper mantle. Contrib. Mineral. Petrol. 114, 331–348.

Berry, A., O'Neill, H., Jayasuriya, K., Campbell, S., Foran, G., 2003. XANES calibrations for the oxidation state of iron in a silicate glass. Am. Mineral. 88, 967–977.

Berry, A., Stewart, G., O'Neill, H.S.C., Mallman, G., Mosselmans, F., 2015. A Reassessment of the Oxidation State of Iron in MORB Glasses. Goldschmidt Abstracts #280.

Berry, A., O'Neill, H., Rowe, M., Mosselmans, F., Rivard, C., 2017. The Oxidation State of Iron in Basaltic Glasses. Goldschmidt Abstracts.

Bevington, P.R., Robinson, D.K., 2003. Data Reduction and Error Analysis. McGraw-Hill.

Bézos, A., Humler, E., 2005. The $Fe^{3+}/\Sigma Fe$ ratios of MORB glasses and their implications for mantle melting. Geochim. Cosmochim. Acta 69, 711–725.

Borisov, A., McCammon, C., 2010. The effect of silica on ferric/ferrous ratio in silicate melts: an experimental study using Mössbauer spectroscopy. Am. Mineral. 95, 545–555.

Bowen, L., DeGrave, E., Reid, D., Graham, R., Edinger, S., 1989. Mössbauer study of a California desert celadonite and its pedogenically-related smectite. Phys. Chem. Miner. 16, 697–703.

Brounce, M., Kelley, K., Cottrell, E., 2014. Variations in $Fe^{3+}/\Sigma Fe$ of Mariana arc basalts and mantle wedge fO_2. J. Petrol. 55, 2513–2536.

Burns, R.G., 1994. Mineral Mössbauer spectroscopy: correlations between chemical shift and quadrupole splitting parameters. Hyperfine Interact. 91, 739–745.

Carmichael, I.S.E., 1991. The redox states of basic and silicic magmas: a reflection of their source regions? Contrib. Mineral. Petrol. 106, 129–141.

Carmichael, I.S., Ghiorso, M.S., 1986. Oxidation-reduction relations in basic magma: a case for homogeneous equilibria. Earth Planet. Sci. Lett. 78, 200–210.

Chambaere, D.G., De Grave, E., Vanleerberghe, R.L., Vandenberghe, R.E., 1984. The electric field gradient at the iron sites in βFeOOH. Hyperfine Interact. 20, 249–262.

Chen, Y.-L., Yang, D.-P., 2007. Mössbauer Effect in Lattice Dynamics: Experimental Techniques and Applications. John Wiley & Sons.

Christie, D.M., Carmichael, I.S.E., Langmuir, C.H., 1986. Oxidation states of mid-ocean ridge basalt glasses. Earth Planet. Sci. Lett. 79, 397–411.

Cottrell, E., Kelley, K.A., 2011. The oxidation state of Fe in MORB glasses and the oxygen fugacity of the upper mantle. Earth Planet. Sci. Lett. 305, 270–282.

Cottrell, E., Kelley, K.A., 2013. Redox heterogeneity in mid-ocean ridge basalts as a function of mantle source. Science 340, 1314–1317.

Cottrell, E., Kelley, K.A., Lanzirotti, A., Fischer, R.A., 2009. High-precision determination of iron oxidation state in silicate glasses using XANES. Chem. Geol. 268, 167–179.

Crabtree, S.M., Lange, R.A., 2012. An evaluation of the effect of degassing on the oxidation state of hydrous andesite and dacite magmas: a comparison of pre-and post-eruptive Fe^{2+} concentrations. Contrib. Mineral. Petrol. 163, 209–224.

Dauphas, N., Roskosz, M., Alp, E., Neuville, D., Hu, M., Sio, C., Tissot, F., Zhao, J., Tissandier, L., Medard, E., Cordier, C., 2014. Magma redox and structural controls on iron isotope variations in Earth's mantle and crust. Earth Planet. Sci. Lett. 398, 127–140.

Davis, F.A. and Cottrell, E. (in revision) Experimental investigation of basalt and peridotite oxybarometers: implications for spinel thermodynamic models and Fe^{3+} compatibility during generation of upper mantle melts. Am. Mineral.

De Grave, E., Van Alboom, A., 1991. Evaluation of ferrous and ferric Mössbauer fractions. Phys. Chem. Miner. 18, 337–342.

De Grave, E., Vanleerberghe, R., Verdonck, L., De Geyter, G., 1984. Mössbauer and infrared spectroscopic studies of Belgian chloritoids. Phys. Chem. Miner. 11, 85–94.

De Grave, E., Verbeeck, A.E., Chambaere, D.G., 1985. Influence of small aluminum substitutions on the hematite lattice. Phys. Lett. A 107, 181–184.

De Grave, E., Van Alboom, A., Eeckhout, S.G., 1998. Electronic and magnetic properties of a natural aegirine as observed from its Mössbauer spectra. Phys. Chem. Miner. 25, 378–388.

Dingwell, D.B., Virgo, D., 1987. The effect of oxidation state on the viscosity of melts in the system Na_2O-FeO-Fe_2O_3-SiO_2. Geochim. Cosmochim. Acta 51, 195–205.

Dyar, M.D., Naney, M.T., Swanson, S.E., 1987. Effects of quench methods on Fe^{3+}/Fe^{2+} ratios: a Mössbauer and wet-chemical study. Am. Mineral. 72, 792–800.

Dyar, M., Agresti, D., Schaefer, M., Grant, C., Stlute, E., 2006. Mössbauer spectroscopy of earth and planetary materials. Annu. Rev. Earth Planet. Sci. 34, 83–125.

Dyar, M., Schaefer, M., Sklute, E., Bishop, J., 2008. Mössbauer spectroscopy of phyllosilicates: effects of fitting models on recoil-free fractions and redox ratios. Clay Miner. 43, 3–33.

Dyar, M.D., Breves, E.A., Emerson, E., Bell, S.W., Nelms, M., Ozanne, M.V., Peel, S.E., Carmosino, M.L., Tucker, J.M., Gunter, M.E., Delaney, J.S., Lanzirotti, A., Woodland, A.B., 2012. Accurate determination of ferric iron in garnets by bulk Mössbauer spectroscopy and synchrotron micro-XANES. Am. Mineral. 97, 1726–1740.

Dyar, M.D., Klima, R.L., Fleagle, A., Peel, S.E., 2013. Fundamental Mössbauer parameters of synthetic Ca-Mg-Fe pyroxenes. Am. Mineral. 98, 1172–1186.

Dyar, M.D., McCanta, M., Breves, E., Carey, C., Lanzirotti, A., 2016. Accurate predictions of iron redox state in silicate glasses: a multivariate approach using X-ray absorption spectroscopy. Am. Mineral. 101, 744–747.
Eeckhout, S.G., De Grave, E., 2003. Evaluation of ferrous and ferric Mössbauer fractions. Part II. Phys. Chem. Miner. 30, 142–146.
Eeckhout, S., De Grave, E., Vochten, R., Blaton, N., 1999. Mössbauer effect study of anapaite, $Ca_2Fe^{2+}(PO_4)^2{\cdot}4H_2O$, and of its oxidation products. Phys. Chem. Miner. 26, 506–512.
Eeckhout, S., Grave, E.D., McCammon, C., Vochten, R., 2000. Temperature dependence of the hyperfine parameters of synthetic P21/c Mg-Fe clinopyroxenes along the $MgSiO_3$-$FeSiO_3$ join. Am. Mineral. 85, 943–952.
Ellwood, B.B., Burkart, B., Rajeshwar, K., Darwin, R.L., Neeley, R.A., McCall, A.B., Long, G.J., Buhl, M.L., Hickcox, C.W., 1989. Are the iron carbonate minerals, ankerite and ferroan dolomite, like siderite, important in paleomagnetism? J. Geophys. Res. Solid Earth 94, 7321–7331.
Fei, Y., Virgo, D., Mysen, B., Wang, Y., Mao, H., 1994. Temperature-dependent electron delocalization in (Mg, Fe) SiO_3 perovskite. Am. Mineral. 79, 826–837.
Fiege, A., Ruprecht, P., Simon, A.C., Bell, A.S., Göttlicher, J., Newville, M., Lanzirotti, T., Moore, G., 2017. Calibration of Fe XANES for high-precision determination of Fe oxidation state in glasses: comparison of new and existing results obtained at different synchrotron radiation sources. Am. Mineral. 102, 369–380.
Frost, B.R., 1991. Introduction to oxygen fugacity and its petrologic importance. Rev. Mineral. Geochem. 25, 1–9.
Frost, D.J., McCammon, C.A., 2008. The redox state of Earth's mantle. Annu. Rev. Earth Planet. Sci. 36, 389–420.
Grocke, S.B., Cottrell, E., de Silva, S., Kelley, K.A., 2016. The role of crustal and eruptive processes versus source variations in controlling the oxidation state of iron in Central Andean magmas. Earth Planet. Sci. Lett. 440, 92–104.
Herzberg, C., Asimow, P., 2015. PRIMELT3 MEGA. XLSM software for primary magma calculation: peridotite primary magma MgO contents from the liquidus to the solidus. Geochem. Geophys. Geosyst. 16, 563–578.
Jayasuriya, K.D., O'Neill, H.S.C., Berry, A.J., Campbell, S.J., 2004. A Mössbauer study of the oxidation state of Fe in silicate melts. Am. Mineral. 89, 1597–1609.
Kelley, K.A., Cottrell, E., 2009. Water and the oxidation state of subduction zone magmas. Science 325, 605–607.
Kelley, K.A., Cottrell, E., 2012. The influence of magmatic differentiation on the oxidation state of Fe in a basaltic arc magma. Earth Planet. Sci. Lett. 329, 109–121.
Kelley, K., Cottrell, E., 2016. Basin-Scale Redox Heterogeneity in MORBs and the Upper Mantle. AGU Fall Meeting Abstracts.
Kress, V.C., Carmichael, I.S.E., 1988. Stoichiometry of the iron oxidation reaction in silicate melts. Am. Mineral. 73, 1267–1274.
Kress, V., Carmichael, I., 1991. The compressibility of silicate liquids containing Fe_2O_3 and the effect of composition, temperature, oxygen fugacity and pressure on their redox states. Contrib. Mineral. Petrol. 108, 82–92.
Lagarec, K., Rancourt, D.G., 1997. Extended Voigt-based analytic lineshape method for determining N-dimensional correlated hyperfine parameter distributions in Mössbauer spectroscopy. Nucl. Instrum. Methods Phys. Res., Sect. B 129, 266–280.
Lange, R.A., Carmichael, I.S.E., 1989. Ferric-ferrous equilibria in Na_2O-FeO-Fe_2O_3-SiO_2 melts — effects of analytical techniques on derived partial molar volumes. Geochim. Cosmochim. Acta 53, 2195–2204.
Leider, H., Pipkorn, D., 1968. Mössbauer effect in MgO: Fe^{+2}; low-temperature quadrupole splitting. Phys. Rev. 165, 494.
McCammon, C., 1998. The crystal chemistry of ferric iron in $Fe_{0.05}Mg_{0.95}SiO_3$ perovskite as determined by Mössbauer spectroscopy in the temperature range 80–293 K. Phys. Chem. Miner. 25, 292–300.
McCammon, C.C., Kopylova, M.G., 2004. A redox profile of the slave mantle and oxygen fugacity control in the cratonic mantle. Contrib. Mineral. Petrol. 148, 55–68.
McCammon, C., Pring, A., Keppler, H., Sharp, T., 1995. A study of bernalite, $Fe(OH)_3$, using Mössbauer spectroscopy, optical spectroscopy and transmission electron microscopy. Phys. Chem. Miner. 22, 11–20.
de Moor, J.M., Fischer, T.P., King, P.L., Botcharnikov, R.E., Hervig, R.L., Hilton, D.R., Barry, P.H., Mangasini, F., Ramirez, C., 2013. Volatile-rich silicate melts from Oldoinyo Lengai volcano (Tanzania): implications for carbonatite genesis and eruptive behavior. Earth Planet. Sci. Lett. 361, 379–390.
Moussallam, Y., Oppenheimer, C., Scaillet, B., Gaillard, F., Kyle, P., Peters, N., Hartley, M., Berlo, K., Donovan, A., 2014. Tracking the changing oxidation state of Erebus magmas, from mantle to surface, driven by magma ascent and degassing. Earth Planet. Sci. Lett. 393, 200–209.
Moussallam, Y., Morizet, Y., Gaillard, F., 2016. H_2O–CO_2 solubility in low SiO_2-melts and the unique mode of kimberlite degassing and emplacement. Earth Planet. Sci. Lett. 447, 151–160.
Mysen, B., 2006. The structural behavior of ferric and ferrous iron in aluminosilicate glass near meta-aluminosilicate joins. Geochim. Cosmochim. Acta 70, 2337–2353.
Mysen, B.O., Dubinsky, E.V., 2004. Melt structural control on olivine/melt element partitioning of Ca and Mn. Geochim. Cosmochim. Acta 68, 1617–1633.
Mysen, B.O., Carmichael, I.S.E., Virgo, D., 1985. A comparison of iron redox ratios in silicate glasses determined by wet-chemical and ^{57}Fe Mössbauer resonant absorption methods. Contrib. Mineral. Petrol. 90, 101–106.
Ottonello, G., Moretti, R., Marini, L., Zuccolini, M.V., 2001. Oxidation state of iron in silicate glasses and melts: a thermochemical model. Chem. Geol. 174, 157–179.
Persoons, R., 1990. Mossbauer studie van de hyperfijn parameters in $Co_xFe_{3-x}O_4$, $0 < x < 0.6$, in het temperatuurgebied boven de verwey transitie (PhD Thesis). Gent State University, pp. V–10.
Putirka, K., 2016. Amphibole thermometers and barometers for igneous systems and some implications for eruption mechanisms of felsic magmas at arc volcanoes. Am. Mineral. 101, 841–858.
Righter, K., Danielson, L.R., Pando, K., Morris, R.V., Graff, T.G., Agresti, D.G., Martin, A.M., Sutton, S.R., Newville, M., Lanzirotti, A., 2013. Redox systematics of Martian magmas with implications for magnetite stability. Am. Mineral. 98, 616–628.
Rossano, S., Behrens, H., Wilke, M., 2008. Advanced analyses of 57Fe Mössbauer data of alumino-silicate glasses. Phys. Chem. Miner. 35, 77–93.
Rossano, S., Balan, E., Morin, G., Bauer, J.P., Calas, G., Brouder, C., 1999. Fe Mössbauer spectroscopy of tektites. Phys. Chem. Miner. 26, 530–538.
Sack, R., Carmichael, I., Rivers, M., Ghiorso, M., 1980. Ferric-ferrous equilibria in natural silicate liquids at 1 bar. Contrib. Mineral. Petrol. 75, 369–376.
Seifert, F., Olesch, M., 1977. Mossbauer spectroscopy of grandidierite, (Mg, Fe) Al_3SiO_9. Am. Mineral. 62, 547–553.
Stagno, V., Frost, D.J., 2010. Carbon speciation in the asthenosphere: experimental measurements of the redox conditions at which carbonate-bearing melts coexist with graphite or diamond in peridotite assemblages. Earth Planet. Sci. Lett. 300, 72–84.
Stagno, V., Ojwang, D.O., McCammon, C.A., Frost, D.J., 2013. The oxidation state of the mantle and the extraction of carbon from earth/'s interior. Nature 493, 84–88.
Van Alboom, A., De Grave, E., 1996. Temperature dependence of the ^{57}Fe Mössbauer parameters in riebeckite. Phys. Chem. Miner. 23, 377–386.
Vandenberghe, R., Verbeeck, A., De Grave, E., Stiers, W., 1986. ^{57}Fe Mössbauer effect study of Mn-substituted goethite and hematite. Hyperfine Interact. 29, 1157–1160.
Virgo, D., Mysen, B., 1985. The structural state of iron in oxidized vs. reduced glasses at 1 Atm: a ^{57}Fe Mössbauer study. Phys. Chem. Miner. 12, 65–76.
Waters, L.E., Lange, R.A., 2016. No effect of H_2O degassing on the oxidation state of magmatic liquids. Earth Planet. Sci. Lett. 447, 48–59.
Wilke, M., Partzsch, G.M., Bernhardt, R., Lattard, D., 2005. Determination of the iron oxidation state in basaltic glasses using XANES at the K-edge. Determination of the iron oxidation state in basaltic glasses using XANES at the K-edge. 220, 143–161.
Zhang, H.L., Solheid, P.A., Lange, R.A., Von Der Handt, A., Hirschmann, M.M., 2015. Accurate determination of $Fe^{3+}/\Sigma Fe$ of andesitic glass by Mössbauer spectroscopy. Am. Mineral. 100, 1967–1977.
Zhang, H.L., Hirschmann, M.M., Cottrell, E., Newville, M., Lanzirotti, A., 2016. Structural environment of iron and accurate determination of $Fe^{3+}/\Sigma Fe$ ratios in andesitic glasses by XANES and Mössbauer spectroscopy. Chem. Geol. 428, 48–58.
Zhang, H., Hirschmann, M., Cottrell, E., Withers, A., 2017. Effect of pressure on $Fe^{3+}/\Sigma Fe$ ratio in a mafic magma and consequences for magma ocean redox gradients. Geochim. Cosmochim. Acta 204, 83–103.